

# Modeling and Control of the Wind Energy Conversion Systems Based on DFIG Under Sub- and Super-Synchronous Operation Modes

K. Bedoud<sup>1,2</sup>, M. Ali-rachedi<sup>3</sup>, R. Lakel<sup>1</sup>, T. Bahi<sup>4</sup>.

<sup>1</sup> Automatic Laboratory and Signals, Badji Mokhtar University, Annaba, Algeria.

<sup>2</sup> Welding and NDT Research Centre (CSC). BP 64 Cheraga, Algeria.

<sup>3</sup> Preparatory School in Sciences and Technics, Annaba, Algeria.

<sup>4</sup> Electrical department, Badji Mokhtar University, Annaba, Algeria.

<sup>1</sup> k.bedoud@csc.dz

**Abstract**— In this work, the modeling and control of the Wind Energy Conversion Systems (WECS) based on doubly fed induction generator (DFIG) are presented. Firstly, we developed the models of the different elements of the conversion chain. After, we consider the vector control strategy of the active and reactive powers in order to ensure an optimum operation. Finally, the dynamic model of a DFIG and wind turbine grid connected system is determined in the dq-synchronous reference frame. The numerical simulation results obtained with Matlab/Simulink software present the behaviors of the sub-synchronous and super-synchronous operation modes.

**Keywords**— wind power generation, doubly fed induction generator, renewable energy, modeling, control.

## I. INTRODUCTION

Today, there is a growing demand for energy. However, to satisfy this demand, the world is heading toward the renewable resources for their several advantages, such as the reduction in dependence on fossil fuel resources and the reduction in carbon emissions to the atmosphere. Furthermore, by using renewable energy we avoid the safety problems caused by atomic power [1], [2]. Among these resources, wind energy has recently become the world's fastest growing source of renewable energy [3]. It has a more important energizing potential and it is the first source of extendable energy, takes priority over all other renewable sources of energy worldwide after the hydraulics [4], [5]. Wind energy is a clean renewable energy source. It has been estimated that roughly 10 million MW of energy is continuously available in the earth's wind [6]. Therefore, their facilities increased considerably in the world because while producing electricity, they do not propagate any gas greenhouse effect [7]. Development of wind electricity conversion system not only saves the energy resources, but also is one of most efficient means of improving the makeup of the energy resources and decreasing the environment pollution [8].

Currently, wind variable speed system based on a doubly fed induction generator (DFIG) is most commonly used in

wind farms. It has its many advantages: a very good energy efficiency, robustness, as well as ease of exploitation and control. In addition, it enables operation to a variable speed  $\pm 30\%$  around the synchronous speed, thus guaranteeing a reduced dimensioning of the static converters [9], [10]. Due to these advantages, the DFIG has generated a lot of curiosity on the part of researchers who have tried to develop strategies to best exploit its strong points [11].

In this work, we present the modeling of the mechanical and electrical parts of the conversion chain in order to control the active and reactive powers, independently; in hypo and hyper synchronous modes. For this, three control strategies are considered: MPP control, control of Rotor Side Converter (RSC) and the control of Grid Side Converter (GSC).

The paper is organized as follows. Section 2, presents the description and the modeling of different elements of the conversion chain. The various control algorithms for an optimal turbine operation and control of active and reactive power will be presented in section 3. The results of simulations obtained for the two modes sub-synchronous and super-synchronous modes will be presented and discussed in Section 4. Finally, the conclusions are established.

## II. DESCRIPTION OF THE SYSTEM STUDY

The wind system studied is illustrated in Fig.1. It is constituted by the turbine, the gearbox and the DFIG. The wind captures the kinetic energy of wind and converts it into a torque that makes turn the blades of the rotor. After that, the DFIG transforms the mechanical power into electric power. The DFIG is connected directly to the grid via its stator but also via its rotor through the intermediary of the static converters to allow an exchange of energy between the network and the DFIG at the speed of synchronism. The two converters, network side and DFIG side are controlled by Pulse Width Modulation (PWM) [12]. Through the bidirectional static converters, the DFIG can work in sub-synchronous and super-synchronous modes. Since the converters are designed for a power of 25-30% of the nominal power of the DFIG [13].

Therefore the losses in the converter are little important, their cost is reduced compared to a variable speed wind turbine stator fueled by power converters. Furthermore, the ability to control the reactive power impose the power factor to the connection point of the DFIG to the grid, are the two major reasons for which this machine is found to produce in high power [14]. The different under models of the two parts: mechanical and electric are described below.

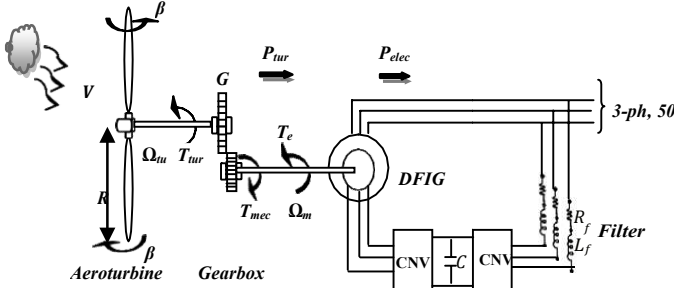


Fig. 1 Schematic diagram of DFIG wind turbine

### II. 1 Wind Turbine Modeling

According that the mechanical system is characterized by the sum of all mechanical characteristics, the Fig.2 show a mechanical model.

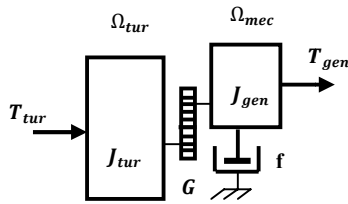


Fig. 2 Mechanical model simplified of wind turbine

The power available from the wind traversing a surface  $S$  is defined by [15].

$$P_v = \frac{1}{2} \cdot \rho \cdot S \cdot V^3 \quad (1)$$

The mechanical power of the wind turbine is:

$$P_{tur} = C_p \cdot \frac{\rho \cdot S \cdot V^3}{2} \quad (2)$$

The evolution of the power coefficient ( $C_p$ ) depends on the blade pitch angle ( $\beta$ ) and the tip-speed ratio ( $\lambda$ ) which is defined as follows:

$$\lambda = \frac{R \cdot \Omega_{tur}}{V} \quad (3)$$

From summaries achieved on a wind of 1.5 MW, the expression of the power coefficient has been approached, for this type of turbine, by the following equation [16]-[18]:

$$C_p = (0.45 - (0.0167(\beta - 2))) \left( \sin \left( \frac{\pi(\lambda + 0.1)}{15.5 - (0.3(\beta - 2))} \right) - (0.00184(\lambda - 3)(\beta - 2)) \right) \quad (4)$$

The aerodynamic torque expression is given by:

$$T_{tur} = \frac{P_{tur}}{\Omega_{tur}} = C_p \cdot \frac{\rho \cdot S \cdot V^3}{2} \cdot \frac{1}{\Omega_{tur}} \quad (5)$$

Fig.3 shows the power rotor speed curves under different wind speeds. We notice that each has a given maximum power point (MPP).

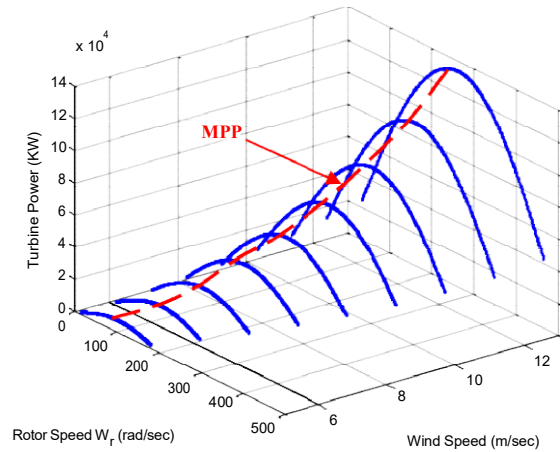


Fig. 3 Turbine power versus rotor speeds and wind speed

The gearbox is installed between the turbine and generator to adapt the speed of the turbine to that of the generator:

$$\Omega_{mec} = G \cdot \Omega_{tur} \quad (6)$$

The friction, elasticity and energy losses in the gearbox are neglected.

$$G = \frac{T_{tur}}{T_{mec}} \quad (7)$$

The dynamic equation is presented by the following relation:

$$J \frac{d\Omega_{mec}}{dt} + f \Omega_{mec} = T_{mec} - T_{em} \quad (8)$$

$$J = \frac{J_{tur}}{G^2} + J_{gen} \quad (9)$$

Fig. 4. Shows the crucial advantage of variable speed wind turbines compared to fixed speed. If the wind speed varies  $V_{w1}$  and  $V_{w2}$  to the speed  $\omega_1$  of the DFIG is unchanged, the power varies from  $P_1$  to  $P_2$ . In addition, the maximum power is equal to  $P_3$ . In case we want to extract the maximum power should be changed by  $\omega_1$  and  $\omega_2$  thus make the variable speed depending on the wind speed. The extraction of maximum

power control is to adjust the torque of the DFIG to extract maximum power. The red dotted line indicates the optimal power points for respectively  $v=8$  m/s and 12 m/s, where the  $C_p$  coefficient is kept at its maximum value.

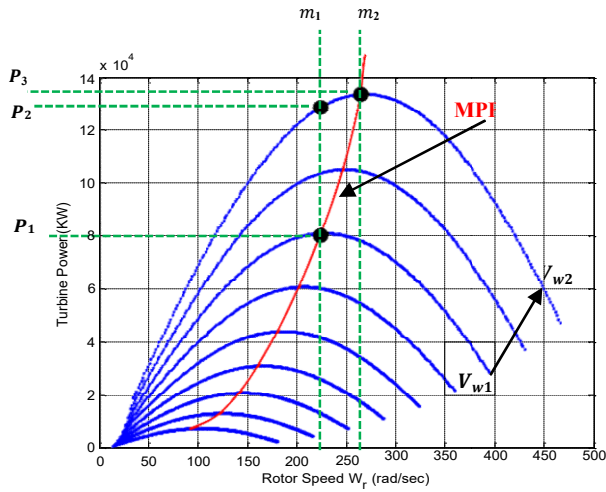


Fig. 4 Turbine power versus rotor speeds of generator

## II. 2 Modeling the DFIG with Stator Field Orientation

For the DFIG modeling, the following assumptions are considered [19], [20]:

- the notching effect is negligible;
- the magnetic saturation is neglected;
- the resistance of the windings is constant;
- the flux distribution is sinusoidal.

The Park model of DFIG is given by the equations below:

$$\begin{cases} V_{sd} = R_s i_{sd} + \frac{d\varphi_{sd}}{dt} - \omega_s \varphi_{sq} \\ V_{sq} = R_s i_{sq} + \frac{d\varphi_{sq}}{dt} + \omega_s \varphi_{sd} \end{cases} \quad (10)$$

$$\begin{cases} V_{rd} = R_r i_{rd} + \frac{d\varphi_{rd}}{dt} - \omega_r \varphi_{rq} \\ V_{rq} = R_r i_{rq} + \frac{d\varphi_{rq}}{dt} + \omega_r \varphi_{rd} \end{cases} \quad (11)$$

As the d and q axis are magnetically decoupled, the stator and rotor flux are given as:

$$\begin{cases} \varphi_{sd} = L_s i_{sd} + L_m i_{rd} \\ \varphi_{sq} = L_s i_{sq} + L_m i_{rq} \end{cases} \quad (12)$$

$$\begin{cases} \varphi_{rd} = L_r i_{rd} + L_m i_{sd} \\ \varphi_{rq} = L_r i_{rq} + L_m i_{sq} \end{cases} \quad (13)$$

The active and reactive powers are defined as:

$$\begin{cases} P_s = V_{sd} i_{sd} + V_{sq} i_{sq} \\ Q_s = V_{sq} i_{sd} - V_{sd} i_{sq} \end{cases} \quad (14)$$

$$\begin{cases} P_r = V_{rd} i_{rd} + V_{rq} i_{rq} \\ Q_r = V_{rq} i_{rd} - V_{rd} i_{rq} \end{cases} \quad (15)$$

Consequently, the d-q orientation has to be synchronized with the stator flux see Fig. 5.

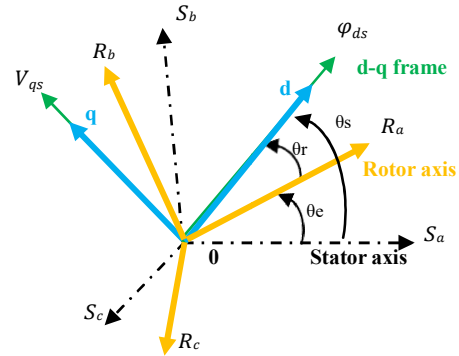


Fig. 5 Orientation of the d-q frame

Within Fig. 5, we can write:

$$\begin{cases} \dot{\theta}_s = \omega_s \\ \dot{\theta}_r = \omega_r \\ \dot{\theta}_e = \omega_e = \omega_s - \omega_r = p\omega_m \end{cases} \quad (16)$$

Defining the slip by:  $g = \frac{\omega_s - \omega_e}{\omega_s}$ .

The Park frame is oriented so that the stator flux will be in quadrature with the q axis ( $\varphi_{qs} = 0$ ,  $\varphi_{ds} = \varphi_s$ ), the equation (12) can be written as follows:

$$\begin{cases} \varphi_{sd} = \varphi_s = L_s i_{sd} + L_m i_{rd} \\ \varphi_{sq} = 0 = L_s i_{sq} + L_m i_{rq} \end{cases} \quad (17)$$

Considering that the resistance of the stator winding ( $R_s$ ) is neglected [21], [22], the voltage and the flux equations of the stator windings can be simplified in steady state as:

$$\begin{cases} V_{sd} = \frac{d\varphi_{sd}}{dt} \\ V_{sq} = \omega_s \cdot \varphi_{sd} \end{cases} \quad (18)$$

The grid is supposed stable with voltage  $v_s$  and synchronous angular frequency ( $\omega_s$ ) constant what implies  $\varphi_{ds} = cst$ .

$$\begin{cases} V_{sd} = 0 \\ V_{sq} = V_s = \omega_s \cdot \varphi_{sd} \end{cases} \quad (19)$$

Hence, the relationship between the stator and rotor currents can be written as follows:

$$\begin{cases} i_{sd} = \frac{\varphi_s}{L_s} - \frac{L_m}{L_s} i_{rd} \\ i_{sq} = -\frac{L_m}{L_s} i_{rq} \end{cases} \quad (20)$$

From the equations (13) and (20), we can write:

$$\begin{cases} \varphi_{rd} = \left( L_r - \frac{M^2}{L_s} \right) i_r + \frac{M V_s}{\omega_s L_s} \\ \varphi_{rq} = \left( L_r - \frac{M^2}{L_s} \right) i_{rq} \end{cases} \quad (21)$$

Replacing the equations (19, 21) in (10, 11) the stator and rotor voltages are then simplified to:

$$\begin{cases} V_{sd} = \frac{R_s}{L_s} \varphi_{sd} - \frac{R_s}{L_s} L_m i_{rd} \\ V_{sq} = -\frac{R_s}{L_s} L_m i_{rq} + \omega_s \varphi_{sd} \end{cases} \quad (22)$$

$$\begin{cases} V_{rd} = R_r i_{rd} + \sigma_r L_r \frac{di_{rd}}{dt} + e_{rd} \\ V_{rq} = R_r i_{rq} + \sigma_r L_r \frac{di_{rq}}{dt} + e_{rq} + e_\varphi \end{cases} \quad (23)$$

Where:

$$\begin{cases} e_r = -\sigma_r L_r \omega_r i_{rq} \\ e_{rq} = \sigma_r L_r \omega_r i_{rd} \\ e_\varphi = \omega_r \frac{M}{L_s} \varphi_{sd} \\ \sigma = 1 - \left( \frac{M}{\sqrt{L_s L_r}} \right)^2 \end{cases} \quad (24)$$

$(L_r - \frac{M^2}{L_s})$ : coupling term between the two axes compensable in the control loop [14] and  $e_\varphi$ : electromotive force.

Taking into consideration the chosen reference frame, the electrical active and reactive powers delivered by the stator and the rotor are given by:

$$\begin{cases} P_s = -\frac{V_s M}{L_s} i_r \\ Q_s = \frac{V_s^2}{L_s \omega_s} - \frac{M V_s}{L_s} i_{rd} \\ P_r = g_r \frac{V_s M}{L_s} i_{rq} \\ Q_r = g_r \frac{V_s M}{L_s} i_{rd} \end{cases} \quad (25)$$

In equation (25),  $Q_s$  divided into two parts: the magnetizing part « $\frac{V_s^2}{L_s \omega_s}$ » and the reactive power exchanged with the grid « $\frac{M V_s}{L_s} i_{rd}$ ».

The electromagnetic torque is as follows:

$$T_{em} = -P_r \frac{M}{L_s} \varphi_{sd} i_{rq} \quad (26)$$

### III. WIND TURBINE CONTROL SYSTEM

In this work, the three controls studied are:

- extraction of the maximum wind power control “MPP” (Maximum Power Point) from the wind for a wide range of wind speeds,
- control of CNV<sub>2</sub>,
- control of CNV<sub>1</sub>.

These controls will be considered separately.

#### III.1 Maximum Power Point Control

Fig. 6 illustrates the principle of MPP control without speed control of the rotation speed:

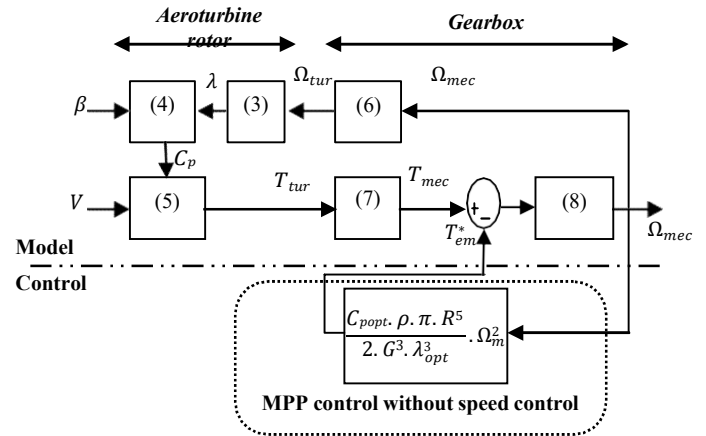


Fig. 6 Block diagram without speed control

The control system of DFIG wind turbine assures the variable speed operation that maximizes the output power for a wide range of wind speeds. The power extracted from the wind is maximized when the rotor speed is such that the power coefficient is optimal  $C_{popt}$ . Therefore, we must set the tip speed ratio on its optimal value  $\lambda_{opt}$ . The electromagnetic torque reference determined by MPP control is thus expressed by the following equation [20]:

$$T_{em}^* = \frac{C_{popt} \cdot \rho \cdot \pi \cdot R^5}{2 \cdot G^3 \cdot \lambda_{opt}^3} \cdot \Omega_m^2 \quad (27)$$

Fig. 7 illustrate  $C_p$  the power coefficient characteristic in function of  $\lambda$  with  $\beta=2^\circ$ . This figure indicates that there is one specific point at which the turbine is most efficient.

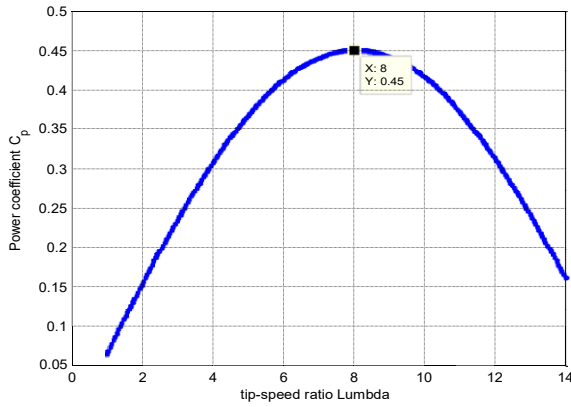


Fig. 7 Power coefficient versus tip speed ratio

III.2 Modeling and Control of the Grid Side Converter CNV<sub>2</sub>

The mathematic model of gird-side converter can be described in matrix form [23]:

$$\begin{bmatrix} \frac{di_{fd}}{dt} \\ \frac{di_{fq}}{dt} \\ \frac{dc}{dt} \end{bmatrix} = \begin{bmatrix} -R_f & 0 & -S_d \\ L_f & -R_f & L_f \\ -\omega_s & L_f & L_f \end{bmatrix} \begin{bmatrix} i_{fd} \\ i_{fq} \\ V_{dc} \end{bmatrix} + \begin{bmatrix} 1 & 0 & 0 \\ L_f & 1 & 0 \\ 0 & 0 & -\frac{1}{C} \end{bmatrix} \begin{bmatrix} e_{fd} \\ e_{fq} \\ V_{dc} \end{bmatrix} \quad (28)$$

Where  $S_q, S_d$  are the switches functions and  $C$  is the capacitance. From the above equation, we can conclude:

$$\begin{cases} L \frac{di_{fd}}{dt} = -R i_{fd} + e_{fd} - S_d V_{dc} \\ L \frac{di_{fq}}{dt} = -R i_{fq} + e_{fq} - S_q V_{dc} \end{cases} \quad (29)$$

Because, the output voltage of the grid-side converter can be set:

$$\begin{cases} V_{fd} = S_d V_{dc} \\ V_{fq} = S_q V_{dc} \end{cases} \quad (30)$$

Where:

$$\begin{cases} e_{fd} = \omega_s L_f i_{fq} + V_{sd} \\ e_{fq} = -\omega_s L_f i_{fd} + V_{sq} \end{cases} \quad (31)$$

The equations indicate that the current feedback  $\omega_s L_f i_{fq}$ ,  $-\omega_s L_f i_{fd}$  can realize decoupling, meantime the gird disturb voltage can carry out forward feed compensation. So the independent control of  $i_{fq}$ ,  $i_{fd}$  can be acquired. The active power and the reactive power of gird-side converter are written as follows [23], [24]:

$$\begin{cases} P = \frac{3}{2} U_m i_{fd} \\ Q = \frac{3}{2} U_m i_{fq} \end{cases} \quad (32)$$

Where  $U_m$  is the amplitude of phase voltage.

The objective of the control of the grid side converter “CNV<sub>2</sub>” is to maintain the tension of the bus “DC” constant regardless of the amplitude and the flow direction of the DFIG rotor power and the regulating of the grid side power factor by controlling the currents flowing in the RL filter. The current  $i_{fq\_ref}$ ,  $i_{fd\_ref}$  are respectively resulting from DC bus control and reactive power at the connection point of CNV<sub>2</sub> with the network.

Where:

$$i_{fd\_ref} = \frac{Q_{f\_ref}}{V_{sq}} \quad (33)$$

$$i_{fq\_ref} = \frac{P_{f\_ref}}{V_{sq}} \quad (34)$$

The block diagram of current control in Park reference frame is illustrated in Fig. 8.

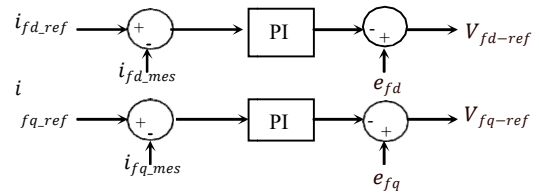


Fig.8 Block diagram of current control(128)

III. 3 Control of the DC Bus

The control of the DC bus voltage allows not only for the reference active power  $P_{c\_ref}$  which is necessary to charge the capacitor to the desired value. But also, the power factor side network can be set through the power reactive. Fig. 9 shows the bloc diagram of DC bus control.

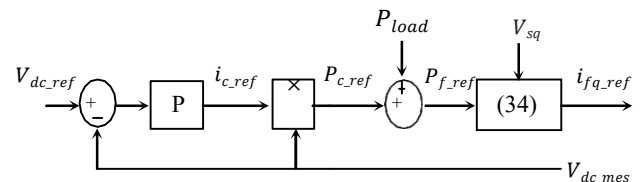


Fig. 9 Bloc diagram of DC bus control.

III.4 Control of the Rotor Side Converter CNV<sub>1</sub>

The rotor side converter “CNV<sub>1</sub>” permits to control active and reactive powers produced by the machine. It’s controlled by acting on the direct and quadrature components of the rotor voltage. This allows the decoupled control of active and reactive powers. Furthermore, the control is obtained by controlling the rotor currents of the DFIG. The model of DFIG in d-q reference frame with stator field orientation shows that the rotor currents can be controlled independently. Fig. 10 shows the bloc diagram of rotor currents control with  $i_{rd\_ref}$ ,  $i_{rq\_ref}$  are given by:

$$\begin{cases} i_{rd\_ref} = \frac{\varphi_{sd}}{M} - \frac{L_s}{M.V_{sq}} \cdot Q_{s\_ref} \\ i_{rq\_ref} = -\frac{L_s}{M.V_{sq}} \cdot P_{s\_ref} \end{cases} \quad (35)$$

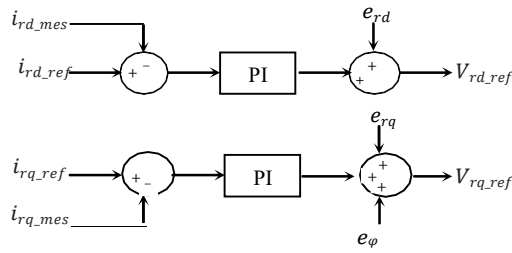


Fig. 10 Bloc diagram of rotor currents control

IV. SIMULATION AND INTERPRETATION

Based on the last study, we present the block diagram of the tested system in following figure. The developed program was used to present the simulation illustrated and discussed for the validity of the study. The simulation parameters are given in table 1 of the appendix A. The studied system has been tested in sub-synchronous and super-synchronous modes.

The Figures 12 and 13 show the simulation results corresponding respectively to the two modes. For this, the unity power factor in the connection of the CNV<sub>2</sub> with the grid is obtained by setting  $Q_{f-ref} = 0$ . Similarly, we vary the stator reactive power  $Q_s$  by varying its reference value in the control of CNV<sub>1</sub>. And, the speed wind 8m/s and 12m/s correspond 1556rd/min and 2336rd/min at the machine speed (see Fig.12a and Fig.13a). All the simulations presented correspond to the changes of the references of active ( $P_s$ ) and reactive ( $Q_s$ ) powers as show in table 2 of the appendix A. Note that for the first time interval (0-0.5s), we held to show the functioning of the wind system with a unity power factor ( $P_{s-ref} = -0.5$  MW and  $Q_{s-ref} = 0$ ).

Concerning the second status, we first change  $Q_s$  at time  $t = 0.5s$  and then  $P_s$  at time  $t = 0.7s$  as shown in the Figures 12b and 13b. We remark that the change of one of these size do not influence the change of the other, which testifies a decoupled control of the active and reactive power, both in sub-synchronous mode (Fig.12. b) and super-synchronous mode (Fig.13.b). However, allow for the functioning of the DFIG in the different quadrants, during the status 3, we changed  $P_{s-ref}$  and  $Q_{s-ref}$  in the opposite sense of the status 2. It is found that the control remain decoupled.

Finally, during the status 4, only  $Q_s$  is changed while keeping  $P_s$  constant. Under these operating conditions, we remark that the power active and reactive to the rotor (see Fig.12.c and Fig.13.c) evolve correctly. However, we notice that since the DFIG needs a reactive power necessary to its magnetization and as the stator reactive power is null ( $Q_s = 0$ ), the DFIG absorbs the reactive power by the rotor.

Fig.12.d and Fig.13.d displays respectively the DC voltage ( $V_{dc}$ ) in sub-synchronous and super-synchronous mode. Furthermore, thanks to the compensation in the implementation control of CV2, It can be seen that  $V_{dc}$  voltage follows perfectly  $V_{dc-ref}$ . In addition, we remark as a light variation of  $V_{dc}$  and that because of the important variation of the rotor reactive power. Knowing that the rotor powers is not uncoupled contrary to the stator powers.

Figures 14 and 15, show the evolution of the stator, rotor and filter currents in sub-synchronous and super-synchronous mode respectively. The currents normally follow the evolutions of the powers previously discussed for the case of stator currents Fig.14a and Fig.15a, whereas the currents to the rotor Fig.14b and Fig.15b evolve identically to the rotor active power in sub-synchronous mode and inversely in super-synchronous mode. Concerning the currents crossing the filter, they remain weak for the case of sub-synchronous mode Fig.14c and Fig.15c and that the current filter on the direct axis is null for the two modes.

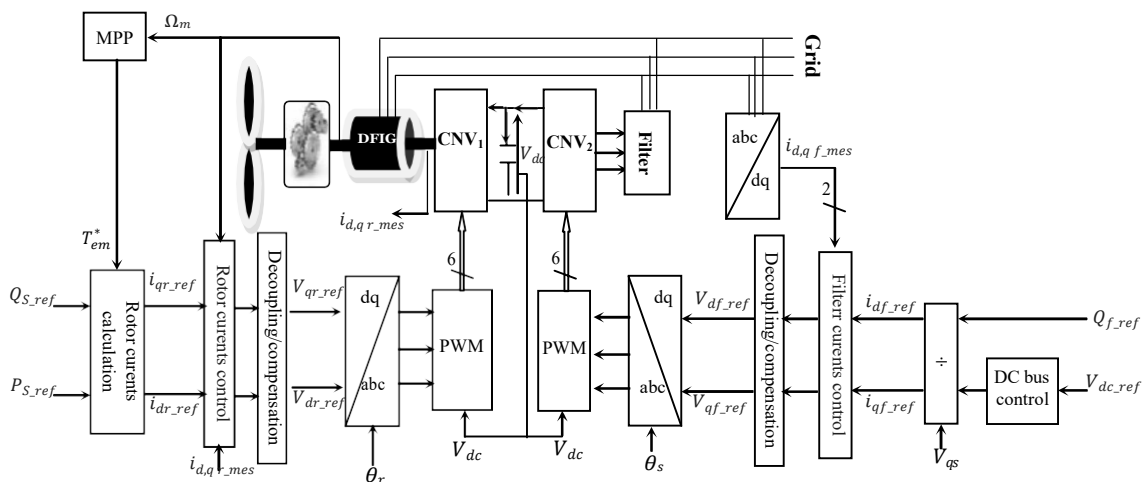


Fig. 11 Block diagram of the control system of the wind

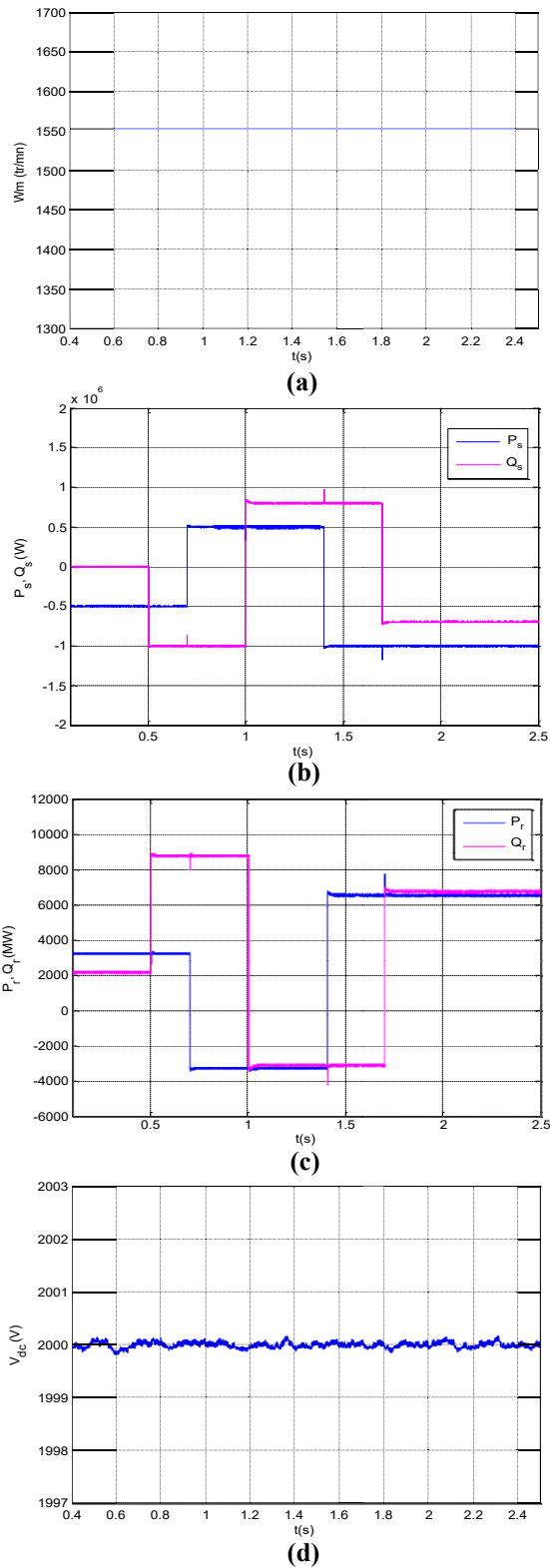


Fig. 12 Sub-synchronous mode

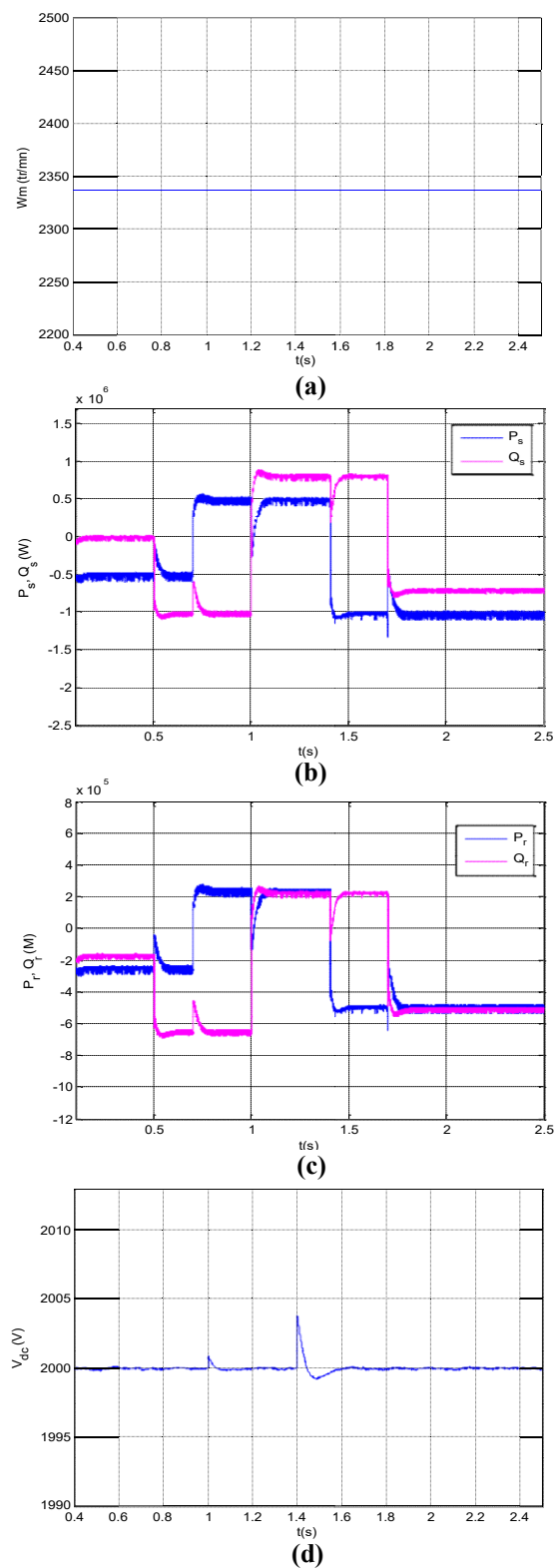
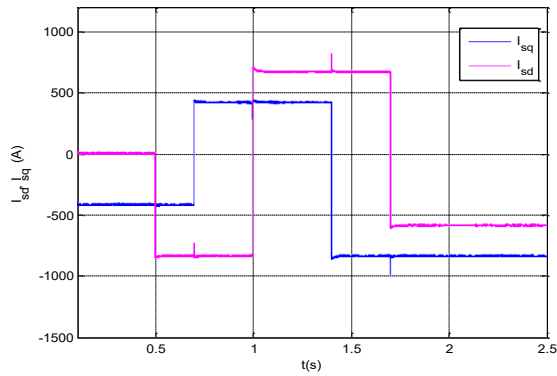
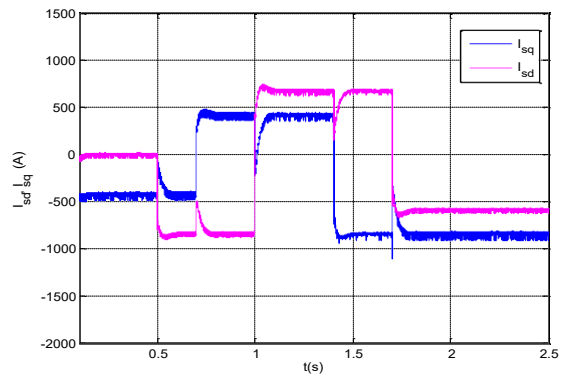


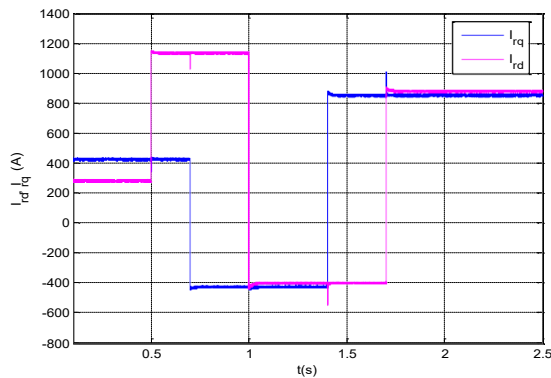
Fig. 13 Super-synchronous mode



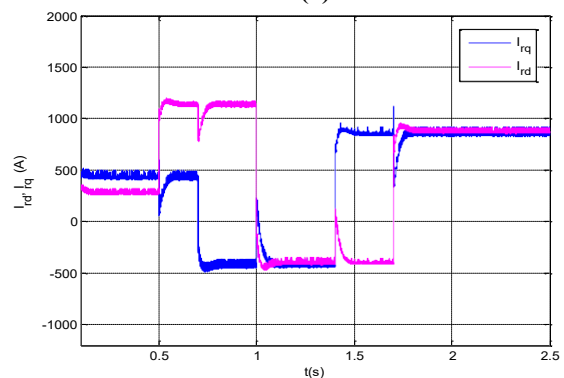
(a)



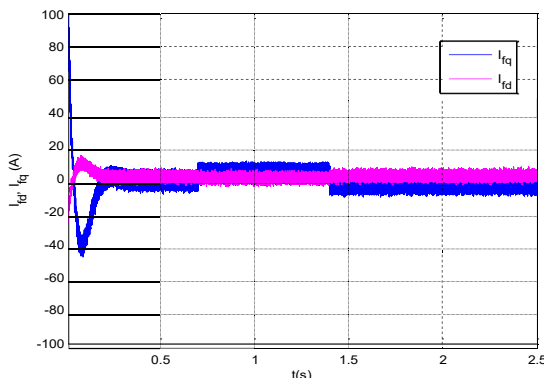
(a)



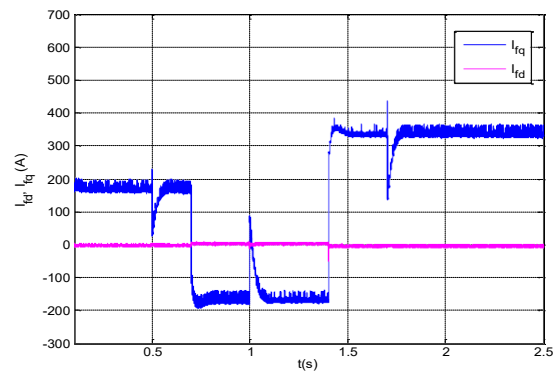
(b)



(b)



(c)



(c)

Fig. 14 Currents d-q axis in sub-synchronous mode

Fig. 15 Currents d-q axis in super-synchronous mode



## APPENDIX A

TABLE I  
FONT SIMULATED DFIG WIND TURBINE PARAMETERS

|                               |                        |
|-------------------------------|------------------------|
| Rated power                   | 1.5MW                  |
| Rotor diameter                | 35.25m                 |
| Gearbox ratio                 | 90                     |
| Friction coefficient : $f$    | 0.0024                 |
| Moment of inertia : $J$       | 1000                   |
| Stator voltage/Frequency      | 690V/50Hz              |
| $R_s / R_r$ ( $\Omega$ )      | 0.012/0.021            |
| $L_m/L_s/L_r$ (H)             | 0.0135/0.0137/0.013675 |
| $R_f$ (H)/ $L_f$ (H)/ $C$ (F) | 0.000002/0.005/0.044   |
| Number of pole pairs: $p$     | 2                      |
| $V_{dc\_ref}$                 | 2000V                  |
| $Q_{f\_ref}$                  | 0                      |

TABLE II  
OPERATION STATUSES OF THE SIMULATED DFIG

| Status | Time (sec)         | Reactive power (MVar) | Time (sec)         | Active power (MW) |
|--------|--------------------|-----------------------|--------------------|-------------------|
| 1      | $0 < t \leq 0.5$   | 0                     | $0 < t \leq 0.7$   | -0.5              |
| 2      | $0.5 < t \leq 1$   | -1                    | $0.7 < t \leq 1.4$ | 0.5               |
| 3      | $1 < t \leq 1.7$   | 0.8                   | $1.4 < t \leq 2.5$ | -1                |
| 4      | $1.7 < t \leq 2.5$ | -0.7                  |                    |                   |

## APPENDIX B

$$\text{MPP control } \begin{cases} \lambda_{opt} = 8. \\ C_{popt} = 0.45. \end{cases}$$

## Controller gains (pu)

For the synthesis of the regulators we opted for the method of poles compensation.

TABLE III  
SYNTHESIS OF THE REGULATORS

| Rotor side converter  | DC bus control  | Grid side converter  |
|---|---|--|
| $t_r = 0.01$ s;<br>$K = \sigma * \frac{L_r}{t_r} = 0.03757$<br>$I = \frac{R_r}{t_r} = 2.10$ | $\xi = 0.707$<br>$t_{r1} = 0.1$ s;<br>$K_c = 2 * \xi * C * \omega_c = 0.16798$<br>$I_c = C * \omega_c^2 = 3.2076$ | $t_{r2} = 2$ ms;<br>$K = \frac{L_f}{t_{r2}} = 25$<br>$I = \frac{R_f}{t_{r2}} = 0.01$ |

## APPENDIX C

TABLE IV  
LIST OF SYMBOLS

|                      |  |
|----------------------|--|
| $P_s, Q_s$           | stator active and reactive power         |
| $P_r, Q_r$           | rotor active and reactive power          |
| $T_{em}$             | DFIG electromagnetic torque (N m)        |
| $d, q$               | synchronous reference frame index        |
| $V_{sd,q}$           | stator d-q frame voltage                 |
| $V_{rd,q}$           | rotor d-q frame voltage                  |
| $i_{sd,q}$           | stator d-q frame current                 |
| $i_{rd,q}$           | rotor d-q frame current                  |
| $\varphi_{sd,q}$     | stator d-q frame flux                    |
| $\varphi_{rd,q}$     | rotor d-q frame flux                     |
| $R_s, R_r$           | stator and rotor Resistances             |
| $L_s, L_r$           | stator and rotor self Inductances        |
| $L_m$                | mutual inductance                        |
| $\omega_s, \omega_r$ | synchronous and rotor angular frequency  |
| $V_{dc}$             | DC link voltage                          |
| $L_f, R_f$           | filter leakage inductance and resistance |
| $\rho$               | air density                              |
| $V_w$                | wind speed                               |
| $R$                  | rotor radius                             |
| $\lambda$            | tip-speed ratio                          |
| $\Omega_t$           | aeroturbine rotor speed                  |
| $\Omega_m$           | generator speed                          |
| $G$                  | gearbox ratio                            |
| $J$                  | turbine total inertia                    |
| $J_{tur}, J_{gen}$   | rotor and DFIG inertia                   |
| $f$                  | turbine total external damping           |
| $i_{load}$           | onduleur current                         |
| $V_{dc\_ref}$        | voltage reference                        |
| $\sigma$             | Coefficient of dispersion.               |
| $CNV_1$              | First converter                          |
| $CNV_2$              | Second converter                         |

## V. CONCLUSIONS

This paper presents a powers control strategy for doubly fed induction generator which provides decoupled control of active and reactive power. However, the fact of the control of these powers separately permits to adjust the power factor of the installation and in consequence obtain better performance.

Therefore, the detailed modeling of the mechanical part of the wind turbine taking into account the characteristics of the blade profile used and the wedging angle, and the mechanical assembly includes the gearbox is presented. According this model, a control algorithm simulation is given in Matlab/Simulink software to investigate the validity of the study. We not that, the simulation results show that the stator active and reactive control powers give a good performance. Hence, the power control strategy is well adapted to this kind of system.

## REFERENCES

- [1] A. Strupczewskim, "Accident risks in nuclear-power plants," *Applied Energy*, vol. 75, issues. 1-2, pp. 79-86, May-June. 2003.
- [2] R. Banos, F. Manzano-Agugliaro, F.G. Montoya, C. Gil, A. Alcayde, J. Gomez, "Optimization methods applied to renewable and sustainable energy : A review," *Renewable and Sustainable Energy Reviews*, vol. 15, pp. 1753-1766, 2011.
- [3] World Wind Energy Association. World Wind Energy Report 2009. [www.wwindea.org/home/images/stories/worldwindenergyreport2009\\_s.pdf](http://www.wwindea.org/home/images/stories/worldwindenergyreport2009_s.pdf), 2010.
- [4] L. P. a. K. E. Johnson, "Control of Wind Turbines," *IEEE Control system magazine*, pp. 44-61, 2011.
- [5] "I.E.A. Statistics. Renewables information with 2009 data," International Energy Agency, OECD/IEA, Paris, 2010.
- [6] Yulin He, Xiping Chen, "Wind turbine generator systems. The supply chain in China: Status and problems," *Renewable Energy*, vol. 34, pp. 2892-2897, April. 2009.
- [7] M.-S. Lu, C.-L. Chang, W.-J. Lee, and L. Wang, "Combining the wind power generation system with energy storage equipment," *IEEE Trans. Ind. Applcat.*, vol. 45, no. 6, pp. 2109-2115, Nov-Dec. 2009.
- [8] Wenyi Liu, Baoping Tang, Yonghua Jiang, "Status and problems of wind turbine structural health monitoring techniques in China: Review," *Renewable Energy*, vol. 35, pp. 1414-1418, 2010.
- [9] Thierno Lamarana Sow, "Nonlinear control of the wind turbine at DFIG for a participation to the regulating of the frequency of the network," Doct. Thesis, Superior technology school, Quebec, Jan. 2012.
- [10] I. Lopez-García, G. Espinosa-Perez, H. Siguerdidjane, A. Doria-Cerezo, "On the passivity-based power control of a doubly-fed induction machine," *International Journal of Electrical Power & Energy Systems*, vol. 45, issue. 1, pp. 303-312, Feb. 2013.
- [11] W. Hofmann, F. Okafor, "Doubly-Fed Full-Controlled Induction Wind Generator for Optimal Power Utilization," in *Proceeding of 4<sup>th</sup> IEEE International Conference on Power Engineering and Drive Systems*, 2001, vol. 1, pp. 355 - 361.
- [12] J. A. Baroudi, V. Dinavahi, A. M. Knight, "A review of power converter topologies for wind generators", *Renewable Energy*, vol. 32, no. 14, pp. 2369-2385, Nov. 2007.
- [13] M. J. Zandzadeh, A.Vahedi, "Modeling and improvement of direct power control of DFIG under unbalanced grid voltage condition," *Electrical Power and Energy Systems*, vol. 59, pp. 58-65, July. 2014.
- [14] F. Poitiers, "Study and control of synchronous generator for using wind energy : Machine asynchrone à Cage Autonome, doubly fed induction generator joined to the network" Doct. thesis, Polytechnic school, Nantes University, France, Dec. 2003.
- [15] B. Beltran, al. Sliding, "Mode power control of variable speed wind energy conversion systems," *IEEE Trans. Energy Conversion*, vol. 23, no. 2, pp. 551-558, 2008.
- [16] E. S. Abdin, W. Xu, "Control design and Dynamic Performance Analysis of a Wind Turbine Induction Generator Unit," *IEEE Trans on Energy Conversion*, vol. 15, no. 1, March. 2000.
- [17] S. El. Aimani, "Modeling of the different technologies of wind turbine integrated in a grid of mean tension," Doct. thesis, central school, University of sciences and technologies, Lille, France, Dec. 2004.
- [18] A. Gaillard, "Wind system based on the DFIG: contribution to the study of the quality of the electric energy and the continuity of service," Doct. thesis, Henri Poincare University, Nancy-I, France, April. 2010.
- [19] Paul-Étienne. Vidal, "Non-linear control of doubly fed induction generator," Doct. Thesis, National polytechnic Institute, Toulouse, France, 2004.
- [20] L.M. Fernandez, C.A. Garcia, F. Jurado, "Comparative study on the performance of control systems for doubly fed induction generator (DFIG) wind turbines operating with power regulation," *Energy*, vol. 33, pp. 1438- 1452, 2008.
- [21] B. Boukhezzer, H. Siguerdidjane, "Nonlinear control with wind estimation of a DFIG variable speed wind turbine for power capture optimization", *Energy Conversion and Management*, vol. 50, pp. 885-892, February. 2009.
- [22] M. Zamanifar, B. Fani, M.E.H. Golshan, H.R. Karshenas, "Dynamic modeling and optimal control of DFIG wind energy systems using DFT and NSGA-II," *Electric Power Systems Research*, vol. 108, pp. 50- 58, 2014.
- [23] X. Yao, C. yi, D. Ying, J. Guo and L. Yang, "The grid-side PWM Converter of the Wind Power Generation System Based on Fuzzy Sliding Mode Control," in proc. *IEE/ASME International Conference on Advanced Intelligent Mechatronics'08*, 2008.
- [24] K. Belmokhtar, M. L. Doumbia, "Modeling and control of wind system based on doubly fed induction generator for supply power to the electricity grid," in *Proc. CIGE'10*, Bechar, Algérie, Nov. 2010. *Journal of Scientific Research*, vol. 2, no 0, pp. 54-62.